Deep convolutional neural network based on CT images of pulmonary nodules in the lungs of adolescent and young adult patients with osteosarcoma

YUN LONG NI[1], XIN CHENG ZHENG[1], XIAO JIAN SHI[1], YE FENG XU[2] and HUA LI[2]

Departments of [1]Radiology and [2]Oncology, Hangzhou Third People's Hospital, Hangzhou, Zhejiang 310009, P.R. China

Received January 28, 2023; Accepted June 5, 2023

DOI: 10.3892/ol.2023.13930

Abstract. The aim of the present study was to explore the diagnostic value of a deep convolutional neural network (DCNN) model for the diagnosis of pulmonary nodules in adolescent and young adult patients with osteosarcoma. For the present study, 675 chest CT images were retrospectively collected from 109 patients with clinically confirmed osteosarcoma who underwent chest CT examination at Hangzhou Third People's Hospital (Hangzhou, China) from March 2011 to February 2022. CT images were then evaluated using the DCNN and manual models. Subsequently, pulmonary nodules of osteosarcoma were divided into calcified nodules, solid nodules, partially solid nodules and ground glass nodules using the DCNN model. Those patients with osteosarcoma who were diagnosed and treated were followed up to observe dynamic changes in the pulmonary nodules. A total of 3,087 nodules were detected, while 278 nodules were missed compared with those determined using the reference standard given by the consensus of three Experienced radiologists., which was analyzed by two diagnostic radiologists. In the manual model group, 2,442 nodules were detected, while 657 nodules were missed. The DCNN model showed significantly higher sensitivity and specificity compared with the manual model (sensitivity, 0.923 vs. 0.908; specificity, 0.552 vs. 0.351; $P<0.05$). In addition, the DCNN model yielded an area under the curve (AUC) value of 0.795 [95% confidence interval (CI), 0.743-0.846], outperforming that of the manual model (AUC, 0.687; 95% CI, 0.629-0.732; $P<0.05$). The film reading time of the DCNN model was also significantly shorter compared with that of the manual model [mean ± standard deviation (SD); 173.25±24.10 vs. 328.32±22.72 sec; $P<0.05$)]. The AUC of calcified nodules, solid nodules, partially solid nodules and ground glass nodules was calculated to be 0.766, 0.771, 0.761 and 0.796, respectively, using the DCNN model. Using this model, the majority of the pulmonary nodules were detected in patients with osteosarcoma at the initial diagnosis (69/109, 62.3%), and the majority of these were found with multiple pulmonary nodules instead of a single nodule (71/109, 65.1% vs. 38/109, 34.9%). These data suggest that, compared with the manual model, the DCNN model proved to be beneficial for the detection of pulmonary nodules in adolescent and young adult patients with osteosarcoma, which may reduce the time of artificial radiograph reading. In conclusion, the proposed DCNN model, developed using data from 675 chest CT images retrospectively collected from 109 patients with clinically confirmed osteosarcoma, may be used as an effective tool to evaluate pulmonary nodules in patients with osteosarcoma.

Introduction

Osteosarcoma is the most common primary bone malignancy in adolescents and young adults (1,2). With the introduction of neoadjuvant and adjuvant chemotherapy, the 5-year survival rate of patients with osteosarcoma has increased from 20% in the 1970s to a range of 60-80% (3-5). However, this improvement has since reached a plateau, where the 5-year survival rate of patients has not further improved over the past 10 years. Lung metastasis is one of the main factors restricting the improvement of patient survival, rendering it the main cause of mortality in patients with osteosarcoma (6,7).

Timely, accurate and comprehensive identification of pulmonary nodules in patients with osteosarcoma is vital for maximizing long-term survival of patients with osteosarcoma (3,4). Chest CT is the preferred imaging method for evaluating the presence of pulmonary metastasis from primary osteosarcoma (3-5,7). However, manual assessment of pulmonary nodules in patients with osteosarcoma is time-consuming and laborious because of the large number of chest CT scans and the long reading time required by the diagnostic physician.

In recent years, the application of artificial intelligence-assisted diagnostic technology in the medical field has been on the rise. One study showed that average accuracy rate by Neural Network Algorithm is 93.5% in a total of 1,000 eyes fundus images from diabetic patients in which 298 eyes were diagnosed as DR by two ophthalmologists (8). A Deep learning (DL) algorithm achieved a voxel-wise area under the curve of 0.94 and a subject-level accuracy of 92% for

Correspondence to: Dr Hua Li, Department of Oncology, Hangzhou Third People's Hospital, 38 West Lake Avenue, Hangzhou, Zhejiang 310009, P.R. China
E-mail: 41316982@qq.com

Key words: osteosarcoma, pulmonary nodules, artificial intelligence, deep convolutional neural Network, CT

endovascular treatment eligibility (9). Another study showed that an algorithm using a convolutional neural network (CNN) was able to fully-automatically extract on a mean 92% of clinically relevant coronary artery segments (10). Therefore, the aim of the present study was to assess the efficacy of the artificial intelligence diagnostic DCNN model for evaluating pulmonary nodules in adolescent and young adult patients with osteosarcoma. In addition, the present study aimed to compare its clinical application value with another manual model.

Materials and methods

The present retrospective study was approved by the Ethics Committee of Hangzhou Third People's Hospital (Hangzhou, China) and the requirement for informed consent was waived. All methods were performed in accordance with expert consensus on data labeling and the quality control of pulmonary nodules was performed in reference to the 'Consensus on the rule and quality control of pulmonary nodule annotation based on thoracic CT' from 2018 (11). The inclusion criteria were as follows: i) All patients were confirmed histologically with osteosarcoma; ii) patients were 9-35 years old; iii) patients underwent thin-slice CT examination, with a slice thickness of ≤3 mm; iv) the diameter range of all nodules was 2-150 mm; and v) there was no obvious cavity in the thin-slice CT images. The exclusion criteria were the following: i) Incomplete lung lobe scan; ii) serious artifacts in the image; iii) missing layers or faults in the image; and iv) the image did not conform to the DICOM 3.0 protocol (12). The images data of chest CT screening diagnosed with osteosarcoma was retrospectively collected from Hangzhou Third People's Hospital (Hangzhou, China) between March 2011 and February 2022. All examinations were performed as part of routine healthcare plans. Disappearance of the small pulmonary nodules was observed for 3 months continuously, with the CT scanning images re-examined once a month to confirm.

A total of 109 adolescent and young adult patients with osteosarcoma underwent a total of 675 chest CT scans using Somatom Definition Edge 64-slice spiral CT, GE Revolution 16-slice spiral CT [General Electric Medical Investment (China) Co., Ltd.] and uCT-510 16-slice CT (Shanghai United Imaging Healthcare Co., Ltd.). The scanning range was from the apex of the lung to the base of the lung, including both chest walls and axilla. The lung window was used for image analysis and the range of thickness of the reconstructed lung window image was 1-3 mm, with the bone algorithm used for reconstruction. The lung window was used for image analysis, with a window width of 1,500 HU and a window level of -400 HU. Chest CT scans were generally divided into the following four stages: i) At the initial diagnosis of osteosarcoma; ii) during preoperative chemotherapy; iii) within 1 year of the end of treatment; and iv) 1 year after the end of treatment. The selection process for patients included in the present study is shown in Fig. 1.

Pulmonary nodule CT image assistance software used in the present study was developed by Shanghai United Imaging Medical Co., Ltd., approved by the National Medical Products Administration and the China Medical AI Certificate III was obtained (certificate no. National Mechanical Note 20213210471). The artificial intelligence software is based on the three-dimensional convolutional neural network method (13). The simple workflow scheme of the DCNN model development is presented in Fig. 2.

According to the random number table method, (14) CT images were divided into groups A and B, which included a total of 140,610 and 136,032 images, respectively. For group A, the DCNN model was used for artificial intelligence-assisted image analysis. The distribution of nodules in the lung was analyzed by artificial intelligence and the nodules were automatically classified into ground glass nodules, solid nodules, solid nodules and calcified nodules. The short-and long-axis diameters of the pulmonary nodules were automatically measured with the units in millimeters (mm). The long-axis diameter was defined as the farthest two-point distance in the maximum cross-sectional space within the nodule. The short-axis diameter was defined as the longest distance perpendicular to the long diameter within the nodule and the reading time was recorded in seconds (sec). The length of total reading time included the time from DCNN model identification time to the completion of diagnostic report. For group B, The manual mode was used, whereby simple manual reading was applied. The junior physicians (XCZ, WTY and LLS) recorded the number, location and size of nodules According to the maximum diameter of the nodules, and to the China National Guideline of Classification, Diagnosis and Treatment for Lung Nodules (2016 version) (15), the nodules were divided into four categories: Ground glass nodules, solid nodules, partially solid nodules and calcified nodules. The density of the ground glass nodules was slightly higher than that of the surrounding lung parenchyma, but the contours of blood vessels and bronchi within the nodules were still visible. All solid nodules were soft tissue density nodules with uniform density and concealed by blood vessels and bronchi. Partially solid nodules were defined as nodules containing both ground glass density and solid soft tissue density, with uneven density. Calcified nodules were defined as round or round (spherical or spherical) well-defined lesions of complete calcium salt deposition within the lung parenchyma. By contrast, The senior diagnosticians (YLN, SDJ and ZTW) issued the diagnostic report based on the written report and personal opinion, the length of total reading time includes the junior physicians reading time to the senior diagnosticians was recorded. The thin-slice chest CT images of patients with osteosarcoma were analyzed by two diagnostic radiologists with the title of chief physician and >10 years of work experience to determine the number and nature of pulmonary nodules. If the judgment results were inconsistent, a third imaging diagnostic physician with the title of associate chief physician or higher rank and >15 years of work experience would act as the arbiter. This procedure was used as the gold standard for the diagnosis of pulmonary nodules in patients with osteosarcoma.

The CT imaging features of the enrolled nodules were labeled in the standard lung window. Each nodule was diagnosed and labeled by two chest imaging diagnostic physicians with >10 years of work experience in a blinded manner. The decision was made by a third imaging expert with the ranking of associate chief physician or above with >15 years of experience before the final summary of opinions was used as the gold standard for nodule diagnosis and labeling. True-positive detection was defined as when the positioning box of pulmonary

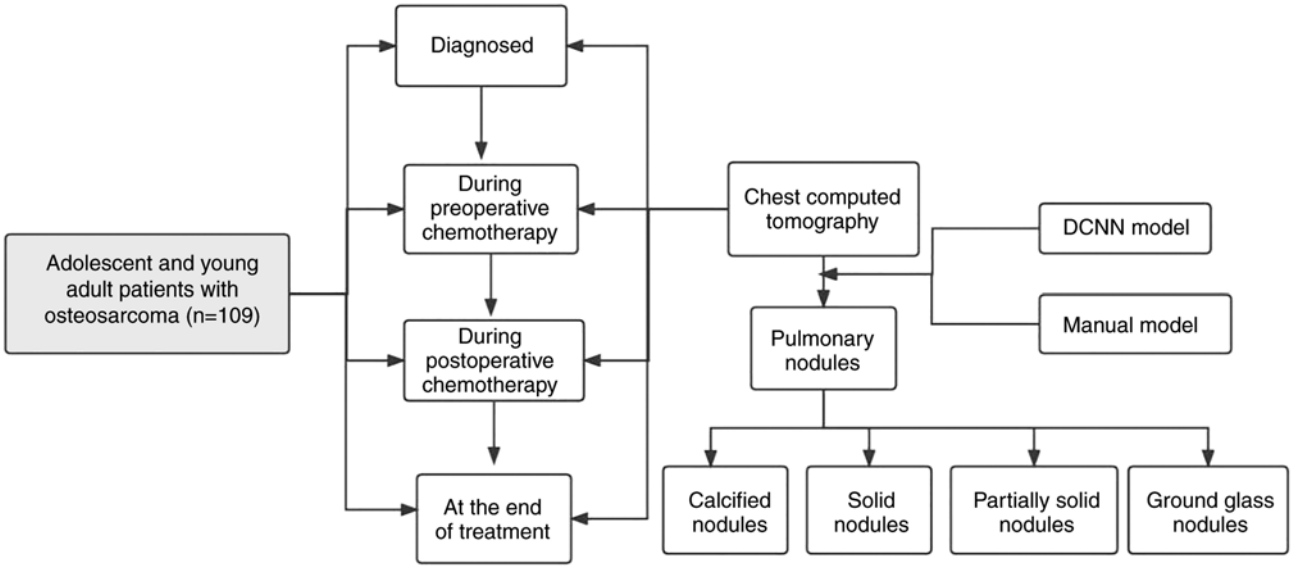

Figure 1. Flow chart of the present study design. DCNN, deep convolutional neural network.

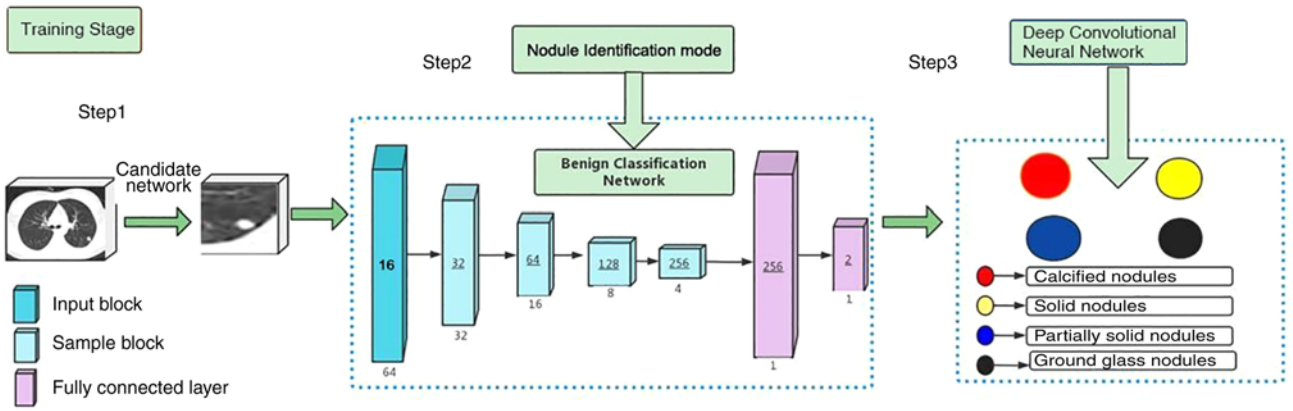

Figure 2. Deep convolutional neural network for assessing pulmonary nodules.

nodules detected by the DCNN model coincided with any of the positioning boxes in the gold standard. Otherwise, the detection of a pulmonary nodule would be considered a false-positive. The following four categories were defined: i) True positive was predicted and observed; ii) true negative was predicted and observed; iii) false negative was observed, but it was predicted; and iv) false positive was observed, but it was predicted. In the present study, the criteria for pulmonary metastasis from the primary osteosarcoma were as follows: i) Pathologically confirmed pulmonary metastasis of osteosarcoma; ii) osteosarcoma pulmonary micrometastasis, whereby thin-slice chest CT was routinely re-examined every 3 months at the beginning, followed by once a month until dynamic changes of pulmonary small nodules were observed; if the small nodules were stable for 12 months, thin-slice chest CT was re-examined every 3 months; iii) intrapulmonary micrometastasis was defined by the enlargement or increase in the number of small nodules in the lung; and iv) ≥ three times of follow-up after diagnosis. The disappearance of small pulmonary nodules was observed continuously for 3 months and CT scan was re-examined once a month.

Statistical analysis. SPSS software (version 18.0; SPSS, Inc.) was used for data analysis and processing, where the adoption rate of count data was expressed in the form of n (%). Data comparison was conducted using the χ^2 test. The unpaired t-test was used to analyze the difference in the reading time between the two groups of samples. The DeLong test was used to compare the diagnostic performance of the two models. Receiver operating characteristic (ROC) curve analysis was applied to compare the predictive performance of the two models. $P<0.05$ was considered to indicate a statistically significant difference.

Results

A total of 109 patients, 65 males and 44 females, with an age range of 9-34 years and median age of 16 years, were included in the present study. All patients were confirmed histologically with osteosarcoma.

Diagnostic performance measurements. Table I presents the evaluation performance of the DCNN and the manual models

for assessing pulmonary nodules in patients with osteosarcoma. In the DCNN model group, 3,087 nodules were detected but 278 nodules were missed compared with the determination using the gold standard, which was performed by two diagnostic radiologists. In the manual model group, 2,442 nodules were detected but 657 nodules were missed. The unpaired t-test was used to analyze the difference in the reading times between the DCNN and the manual model groups.

The reading time of the DCNN model was significantly shorter compared with that of the manual model group [mean ± standard deviation (SD); 173.25±24.10 vs. 328.32±22.72 sec; P<0.05; Table I]. The DeLong test was used to compare the diagnostic performance of the two models. ROC curve analysis was applied to compare the predictive performance of the two models. The area under the ROC curve in the DCNN model group was 0.795 (95% CI, 0.743-0.846), outperforming that of the manual model (AUC, 0.687; 95% CI, 0.629-0.732; P<0.05; Fig. 3). The ROC curve analysis indicated that the DCNN-based model was superior compared to the manual model. The χ^2 test was used to compare the sensitivity and specificity of the DCNN and manual models. The DCNN model had significantly higher sensitivity and specificity compared with the manual model (sensitivity, 0.923 vs. 0.908, respectively; specificity, 0.552 vs. 0.351, respectively; P<0.05).

Nodules characteristics based on the DCNN model. Table II indicates that among the 3,087 nodules detected by the DCNN model, the number of calcified nodules, solid nodules, partially solid nodules and ground glass nodules was 744, 1,540, 206 and 597, respectively, whereas the AUC was 0.766, 0.771, 0.761 and 0.796, respectively (Fig. 4). Table II also presents the diameter, classification and distribution of the pulmonary nodules in the DCNN model.

Dynamically evaluated by the DCNN model. The DCNN model was used to dynamically evaluate and analyze 675 chest CT images of 109 adolescent and young adult patients with osteosarcoma. The DCNN model indicated that >50% of the pulmonary nodules existed at the initial diagnosis (62/109; 58.0%), where cases with multiple pulmonary nodules tended to be more common compared with those with only single pulmonary nodules (68/109, 62.4% vs. 41/109, 37.6%; Table III). At diagnosis, during preoperative chemotherapy, during postoperative chemotherapy and at the end of all treatments, A total of 40 patients exhibited dynamic changes in the pulmonary nodules; among them, the number of pulmonary nodules increased in 17 patients, the diameter of pulmonary nodules increased in 15 patients, the size and number of pulmonary nodules did not change but the density of pulmonary nodules increased in 5 patients, and the number of pulmonary nodules decreased in 3 patients. Finally, 33 patients were diagnosed with pulmonary metastases(Figs. 5, S1 and S2 and Table III). Among them, 16 cases occurred at the time of diagnosis of osteosarcoma, 8 cases of pulmonary metastasis occurred during preoperative chemotherapy, 5 cases during postoperative chemotherapy and 4 cases occurred at the end of all treatment. The DCNN model indicated that the diameter of the majority of the pulmonary nodules was <5 mm (2,434/3,087, 78.8%). Based on density analysis, solid nodules accounted for 50% of the total nodules, whereas calcified nodules and ground glass nodules ranked in the second (21.3%) and third places (20.3%), followed by part-solid nodules. Pulmonary nodules were randomly distributed in either the left or right lobes (Table II).

Table I. DCNN and manual model performance in a cohort of 109 patients with osteosarcoma.

	Testing cohort	
Performance	DCNN model	Manual model
True positives	3,087	2,442
True negatives	343	355
False positives	257	246
False negatives	278	657
Sensitivity	0.923	0.908
Specificity	0.552	0.351
Area under the curve	0.795	0.687
95% confidence interval	(0.743-0.846)	(0.629-0.732)
Reading time (sec)	173.25±24.10	328.32±22.72
P-value	<0.05	

DCNN, deep convolutional neural network.

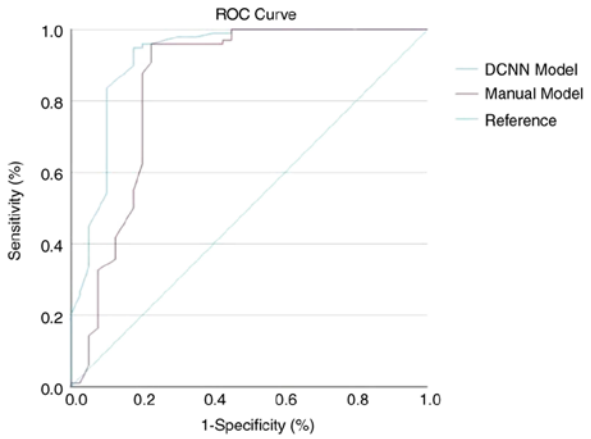

Figure 3. ROC curves of the DCNN and manual models on the testing dataset (n=109). The reference line refers to the ROC Space baseline, a random classifier that predicts 1 with probability of positivity. ROC, receiver operating characteristic; DCNN, deep convolutional neural network.

Discussion

The purpose of the present study was to evaluate the ability of artificial intelligence-assisted technology to identify pulmonary nodules in patients with osteosarcoma. Furthermore, the present study aimed to monitor the dynamic changes in small nodules of ≤5 mm in diameter in the lungs of patients with osteosarcoma using such technology. Patients with osteosarcoma were found to have a higher incidence of pulmonary small nodules (76.9%), where a portion of the pulmonary nodules was diagnosed as lung metastases with dynamic changes (13.4%; 16/119). During the regular follow-up of patients with osteosarcoma, the number and density of pulmonary small nodules may

Table II. Indicators of pulmonary nodules detected by the deep convolutional neural network.

Variable	Nodules ≤5 mm (n=2,434)	Nodules >5 mm (n=653)
Size, mm		
5	307 (12.6)	N/A
4	577 (23.7)	N/A
3	1,083 (44.5)	N/A
2	467 (19.2)	N/A
>20	N/A	60 (9.2)
16-20	N/A	97 (14.8)
11-15	N/A	161 (24.7)
6-10	N/A	335 (51.3)
Calcified nodules	518 (21.3)	226 (34.6)
Solid nodules	1,287 (52.9)	253 (38.7)
Partially solid nodules	135 (5.5)	71 (10.9)
Ground glass nodules	494 (20.3)	103 (15.8)
Right upper lobe	567 (23.3)	101 (15.5)
Right middle lobe	195 (8.0)	57 (8.7)
Right lower lobe	604 (24.8)	185 (28.3)
Left upper lobe	528 (21.7)	129 (19.8)
Left lower lobe	540 (22.2)	181 (27.7)

N/A, not available.

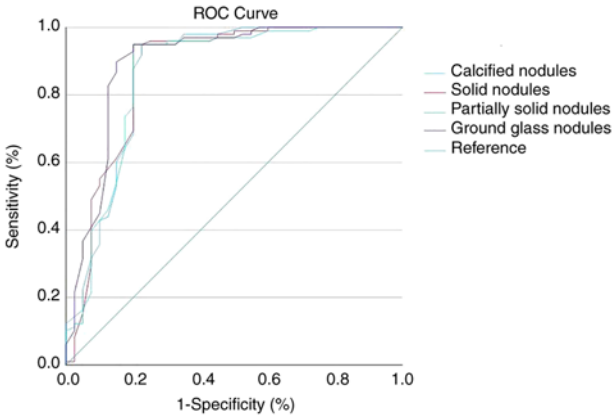

Figure 4. ROC curves of the different types of pulmonary nodules testing with the deep convolutional neural network model (n=109). The number of calcified nodules, solid nodules, partially solid nodules and ground glass nodules was 744, 1,540, 206 and 597 respectively as detected by the DCNN Model, whereas the ROC was 0.766, 0.771, 0.761 and 0.796. ROC, receiver operating characteristic; DCNN, deep convolutional neural network.

increase or decrease, disappear or remain stable. The enlargement or increase of pulmonary small nodules, the increase or decrease of nodule density and the decrease or disappearance of pulmonary small nodules were defined as the dynamic changes of pulmonary small nodules. The possibility of pulmonary metastasis was considered, especially the enlargement or increase of pulmonary small nodules and the increase of nodule density were more likely to be pulmonary metastasis. In addition, 50% of the patients were shown to have small pulmonary metastatic nodules at the time of diagnosis, whilst others were identified during treatment and follow-up. Therefore, long-term dynamic monitoring of small pulmonary nodules throughout the diagnostic and treatment process is pivotal.

Deep learning algorithms are becoming increasingly recognized as a promising technology for application in the medical field (16,17). Zhang *et al* (18) previously applied a deep learning algorithm for the detection of pulmonary nodules, and they found that the trained sensitivity and specificity of the model was 84.4% (95% CI, 80.5-88.3%) and 83.0% (95% CI, 79.5-86.5%), respectively. Subgroup analysis of smaller nodules of <10 mm indicated significant sensitivity and specificity, similar to those of larger nodules with a size range of 10-30 mm. In another study, Nibali *et al* (19) used DCNN for detecting lung nodules, which yielded a sensitivity and specificity of 91.7 and 88.6%, respectively. The present study found that artificial intelligence algorithms may be used to automatically monitor the size, number, location and density of pulmonary nodules in patients with osteosarcoma. Therefore, using thin-slice chest CT and artificial intelligence-assisted technology to dynamically observe the nature of microscopic nodules in the lungs of patients with osteosarcoma appears to be a viable method for improving the diagnostic efficiency for radiologists.

The most commonly applied screening method for osteosarcoma lung metastases is CT, which may improve the sensitivity and specificity for the detection of lung space-occupying lesions. CT scans are not complex and relatively straightforward to perform, and they may be used to detect small pulmonary nodules early to avoid other invasive examinations such as thoracoscopy, bronchoscopy and CT-guided needle biopsy. Tsuchiya *et al* (20) acknowledged that CT scans may detect small pulmonary nodules <5 mm in diameter, in addition to detecting pulmonary nodules with a thickness of 10 mm. Since there can be omissions during CT screening, fine scanning of small nodules should be performed (21). Iwano *et al* (22) showed that a slice thickness of 1 mm was more accurate for identifying benign and malignant solitary pulmonary nodules. With the advent of fine tomographic CT, the detection rate of sub-cm nodules is increasing. Brader *et al* (23) reported that of the 117 nodules in patients with osteosarcoma tested, 80 (68%) were pathologically malignant and 37 (32%) were benign. Specifically, the assessors correctly classified 93-94% of the malignant nodules. However, for benign lesions, the results were more inaccurate and the assessors were only able to correctly classify 11-30% of them. The majority of benign lesions were classified by the assessors to be indeterminate (54-65%), but of a nodule size of 5 mm, and the presence of calcification was found to be associated with an increased likelihood of malignancy (P<0.05). Ghosh *et al* (24) previously classified osteosarcoma nodules into the following three categories: i) No lung metastases; ii) indeterminate nodules; and iii) metastatic nodules. The survival of patients with indeterminate pulmonary nodules was significantly improved compared with that of patients with metastatic disease but survival was similar to that of patients without lung metastases, with metastatic nodules tending to be >5 mm. However, the authors then argued that indeterminate nodules remain a clinical and diagnostic challenge. In recent years, artificial

Table III. Clinical data of 109 patients with osteosarcoma and results of the dynamic monitoring of pulmonary nodules using the deep convolutional neural network model.

Parameter	Value
Age, years	16 (9-34)
Sex	
Male	69 (63.3)
Female	40 (36.7)
Site	
Limb	102 (93.6)
Non-limb	7 (6.4)
Diagnosed	
Dynamic	19 (30.6)
Dynamic (diagnosed metastases)	16
Stability	43 (69.4)
During preoperative chemotherapy	
Dynamic	9 (39.1)
Dynamic(diagnosed metastases)	8
Stability	14 (60.9)
During postoperative chemotherapy	
Dynamic	7 (46.7)
Dynamic (diagnosed metastases)	5
Stability	8 (53.3)
At the end of all treatment	
Dynamic	5 (55.6)
Dynamic(diagnosed metastases)	4
Stability	4 (44.4)
Nodules (type not defined)	
Single	41 (37.6)
Multiple	68 (62.4)

Values are expressed as the median (range) or n (%).

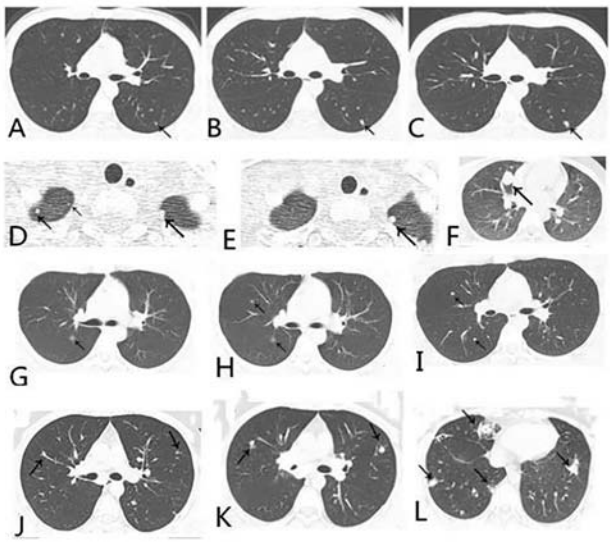

Figure 5. Deep convolutional neural network model for evaluating the dynamic changes of pulmonary nodules in adolescent and young adult patients with osteosarcoma. (A) A solitary pulmonary nodule was found when osteosarcoma was diagnosed by the DCNN model. (B) The nodule was increased in size two and a half months later. (C) Surgical pathology confirmed pulmonary metastasis. (D) During preoperative chemotherapy, Multiple nodules in the lung were found. (E) The nodules were enlarged three months later. (F) Half a year later, multiple nodules in both lungs were diagnosed as pulmonary metastasis. (G) During postoperative chemotherapy, A solitary ground-glass nodules was found in Dorsal segment of the lower lobe of the right lung. (H) Three months later, The nodule was no significant change in this nodule and a new nodule appeared in the upper lobe of the right lung. (I) The two nodules reduced in size but the density increased half a year later. The two nodules were confirmed histologically with osteosarcoma. (J) Based on the DCNN model, Multiple small nodules in both lungs were found at diagnosed osteosarcoma. (K) Multiple nodules were further enlarged and increased during postoperative chemotherapy. (L) Multiple nodules were obviously enlarged and increased at the end of all treatments; lung biopsy confirmed pulmonary metastasis. DCNN, deep convolutional neural network.

intelligence-assisted technology has been used for thoroughly evaluating pulmonary nodules, yielding promising evaluation results for judging the nature of uncertain pulmonary nodules (17,25). In the present study, the application of artificial intelligence-assisted technology for dynamic monitoring indicated that 95 patients with osteosarcoma had pulmonary small nodules (87.1%), while 40 patients with osteosarcoma showed dynamic changes in the pulmonary nodules (36.7%) and 33 (82.5%) were diagnosed with lung metastases during the treatment period, comprising the time windows of diagnosis, neoadjuvant chemotherapy, adjuvant chemotherapy and after all treatments. Previous studies have found lung metastases at the initial diagnosis of all high-grade III osteosarcoma to be ~20% (26). In the present study, lung metastases at the initial diagnosis of high-grade III osteosarcoma were found to be ~50%. There may be several reasons behind this finding. First, The detection rate of pulmonary small nodules based on DCNN model was higher than that based on the manual model, which caused a statistical difference. Previous studies were based on all age groups. The present study focused on adolescents and young adults (9-34 years old). Furthermore, artificial intelligence may quickly identify nodules and shorten the reading time. However, the sensitivity of artificial intelligence technology for pulmonary nodules is high, but the accuracy still needs to be further improved. However, in the current study, the identification of small nodules was based on the evaluation of CT images rather than on histological diagnosis, and diagnostic accuracy of pulmonary nodules is difficult to evaluate by imaging evaluation. In addition, it is likely that in addition to metastasis, microscopic nodules in the lungs of patients with osteosarcoma may also present with various conditions, such as inflammation, hemorrhage and lymph node inflammation.

Determining the nature of small osteosarcoma nodules, benign or metastatic, is a difficult challenge for medical imaging. The artificial intelligence-based DCNN model was therefore developed to evaluate pulmonary nodules. With the advent of fine-slice CT, the detection of sub-cm nodules is increasing. Artificial intelligence can quickly identify nodules and shorten the reading time. In addition, during the follow-up re-examinations of small nodules, artificial intelligence can accurately detect any changes in nodules, such as size enlargement or reduction, and increase or decrease in quantity. In general, the increase and/or increase in pulmonary nodule

size is associated with an increased probability of nodules being metastases. Artificial intelligence classified pulmonary nodules into four categories: Calcified nodules, solid nodules, partially solid nodules and ground glass nodules. The majority of osteosarcoma metastases were calcified nodules and solid nodules. The increase in calcified nodules and solid nodules indicates an increased probability of metastasis. A limitation of this study is that small nodules metastasis of osteosarcoma were diagnosed based on artificial intelligence technology rather than histopathological diagnosis. Traditionally, the gold standard for the diagnosis of pulmonary nodules as osteosarcoma metastasis is not typically the judgement made by the physician, but is instead possible following resection and pathological analysis. The methods used to accurately identify the micrometastatic nodules of osteosarcoma require further study by medical imaging experts. However, with further data support or improvement of imaging techniques, such as MRI/positron emission tomography (PET) or PET/CT (27,28), it is expected to be possible in the future to distinguish small metastatic from benign nodules.

To conclude, artificial intelligence-assisted diagnostic technology may be beneficial for the evaluation and monitoring of pulmonary nodules in patients with osteosarcoma. For patients with osteosarcoma, minute pulmonary nodules with a diameter of <5 mm are frequently found. For patients with osteosarcoma and with small nodules in the lungs, artificial intelligence-assisted diagnosis technology may assist in evaluating whether it is a lung metastasis to timely modify the chemotherapy regimen or to determine the timing of surgery for lung metastases. This may improve the long-term survival rate of patients. However, further research remains necessary.

Acknowledgements

Not applicable.

Funding

The present study was supported by Hangzhou Science and Technology Foundation (grant no. 2020123Y028 and the Natural Science Foundation of Zhejiang Province (grant no. LQ18H290001).

Availability of data and materials

The datasets used and/or analyzed during the current study are available from the corresponding author on reasonable request.

Authors' contributions

YLN, XCZ and HL confirm the authenticity of all the raw data. YLN and HL conceived and designed the study, developed the methodology used and drafted the original manuscript. XCZ curated the data and carried out the formal analysis. XJS visualized the data and participated in the investigation. YLN, YFX and HL conducted deep learning modeling and statistical analysis based on data. HL validated and revised the final manuscript. All authors have read and approved the final version of the manuscript.

Ethics approval and consent to participate

The present study involving human participants was reviewed and approved by the Medical Ethics Committee of Hangzhou Third People's Hospital (Hangzhou, China). Written informed consent for participation was not required for the current study in accordance with the national legislation and institutional requirements.

Patient consent for publication

Not applicable.

Competing interests

The authors declare that they have no competing interests.

References

1. Whelan J, Seddon B and Perisoglou M: Management of osteosarcoma. Curr Treat Option Oncol 7: 444-455, 2006.
2. Picci P: Osteosarcoma (Osteogenic sarcoma). Orphanet J Rare Dis 2: 1-4, 2007.
3. Giger ML, Bae KT and Macmahon H: Computerized detection of pulmonary nodules in computed tomography images. Invest Radiol 29: 459-465, 1994.
4. Schaner EG, Chang AE, Doppman JL, Conkle DM, Flye MW and Rosenberg SA: Comparison of computed and conventional whole lung tomography in detecting pulmonary nodules: A prospective radiologic-pathologic study. Am J Roentgenol 131: 51-54, 1978.
5. Obata H, Kuratsu S, Uchida A, Araki N, Myoui A, Ueda T and Yoshikawa H: Analysis of organ selectivity in the metastatic behavior of Dunn osteosarcoma. Clin Orthop Relat Res 398: 212-222, 2002.
6. Ciccarese F, Bazzocchi A, Ciminari R, Righi A, Rocca M, Rimondi E, Picci P, Reggiani MLB, Albisinni U, Zompatori M and Vanel D: The many faces of pulmonary metastases of osteosarcoma: Retrospective study on 283 lesions submitted to surgery. Eur J Radiol 84: 2679-2685, 2015.
7. Nakajima J, Murakawa T, Fukami T, Sano A, Sugiura M and Takamoto S: Is finger palpation at operation indispensable for pulmonary metastasectomy in colorectal cancer? Ann Thorac Surg 84: 1680-1684, 2007.
8. Cao K, Xu J and Zhao WQ: Artificial intelligence on diabetic retinopathy diagnosis: An automatic classification method based on grey level co-occurrence matrix and naive Bayesian model. Int J Ophthalmol 12: 1158-1162, 2019.
9. Wang K, Shou Q, Ma SJ, Liebeskind D, Qiao XJ, Saver J, Salamon N, Kim H, Yu Y, Xie Y, *et al*: Deep learning detection of penumbral tissue on arterial spin labeling in stroke. Stroke 51: 489-497, 2020.
10. Wolterink JM, van Hamersvelt RW, Viergever MA, Leiner T and Išgum I: Coronary artery centerline extraction in cardiac CT angiography using a CNN-based orientation classifier. Med Image Anal 51: 46-60, 2019.
11. National Institutes for Food and Drug Control, Cardio-thoracic Working Group, Chinese Society of Radiology, Chinese Medical Association: Expert consensus on the rule and quality control of pulmonary nodule annotation based on thoracic CT. Chin J Radiol 53: 9-15, 2019 (In Chinese).
12. Drnasin I, Grgić M and Gogić G: JavaScript access to DICOM network and objects in web browser. J Digit Imaging 30: 537-546, 2017.
13. Huang Y, Ahmad S, Fan J, Shen D and Yap PT: Difficulty-aware hierarchical convolutional neural networks for deformable registration of brain MR images. Med Image Anal 67: 101817, 2021.
14. Sarmah BK and Chakrabarty D: Examination of proper randomness of the numbers generated by rand corporation (1955) random number table: t-Test. 2015.DOI:10.15680/IJIRSET.2015.0410007.
15. Zhou Q, Fan Y, Wang Y, Qiao Y, Wang G, Huang Y, Wang X, Wu N, Zhang G, Zheng X and Bu H: China national guideline of classification, diagnosis and treatment for lung nodules (2016 Version). Zhongguo Fei Ai Za Zhi 19: 793-798, 2016 (In Chinese).

16. Ardila D, Kiraly AP, Bharadwaj S, Choi B, Reicher JJ, Peng L, Tse D, Etemadi M, Ye W, Corrado G, *et al*: End-to-end lung cancer screening with three-dimensional deep learning on low-dose chest computed tomography Nat Med 25: 954-961, 2019.
17. Massion PP, Antic S, Ather S, Arteta C, Brabec J, Chen H, Declerck J, Dufek D, Hickes W, Kadir T, *et al*: Assessing the accuracy of a deep learning method to risk stratify indeterminate pulmonary nodules. Am J Respir Crit Care Med 202: 241-249, 2020.
18. Zhang C, Sun X, Dang K, Li K, Guo XW, Chang J, Yu ZQ, Huang FY, Wu YS, Liang Z, *et al*: Toward an expert level of lung cancer detection and classification using a deep convolutional neural network. Oncologist 24: 1159-1165, 2019.
19. Nibali A, He Z and Wollersheim D: Pulmonary nodule classification with deep residual networks. Int J Comput Assist Radiol Surg 12: 1799-1808, 2017.
20. Tsuchiya H, Kanazawa Y, Abdel-Wanis ME, Asada N, Abe S, Isu K, Sugita T and Tomita K: Effect of timing of pulmonary metastases identification on prognosis of patients with osteosarcoma: The Japanese musculoskeletal oncology group study. J Clin Oncol 20: 3470-3477, 2002.
21. Briccoli A, Rocca M, Salone MC, Fiore MD, Vanel D, Balladelli A and Alberghini M: 'Bubble-like' lung metastases in osteosarcoma patients. Eur J Radiol 71: 144-146, 2009.
22. Iwano S, Makino N, Ikeda M, Itoh S, Tadokoro M, Satake H and Ishigaki T: Solitary pulmonary nodules: Optimal slice thickness of high-resolution CT in differentiating malignant from benign. Clin Imaging 28: 322-328, 2004.
23. Brader P, Abramson SJ, Price AP, Ishill NM, Emily ZC, Moskowitz CS, La Quaglia MP and Ginsberg MS: Do characteristics of pulmonary nodules on computed tomography in children with known osteosarcoma help distinguish whether the nodules are malignant or benign? J Pediatr Surg 46: 729-735, 2011.
24. Ghosh KM, Lee LH, Beckingsale TB, Gerrand CH and Rankin KS: Indeterminate nodules in osteosarcoma: What's the follow-up? Brit J Cancer 118: 634-638, 2018.
25. Xiao Q, Gu Y, Wu J, Wang Z and Huang Y: Abstract P6-02-19: Machine learning based analysis of CT radiomics for the simultaneous indeterminate pulmonary nodules of breast cancer. Cancer Res 79: P6-02-19-P6-02-19, 2019.
26. Zhang C, Guo X, Xu Y, Han X, Cai J, Wang X and Wang G: Lung metastases at the initial diagnosis of high-grade osteosarcoma: Prevalence, risk factors and prognostic factors. A large population-based cohort study. Sao Paulo Med J 137: 423-429, 2019.
27. Susam S, Cinkooglu A, Ceylan KC, Gürsoy S, Kömürcüoğlu BE, Mertoğlu A, Çırak AK, Tuksavul F, Gayaf M, Güldaval F, *et al*: Diagnostic success of transthoracic needle biopsy and PET-CT for 1 to 2 cm solid indeterminate pulmonary nodules. Clin Respir J 14: 453-461, 2020.
28. Grisanti F, Zulueta J, Rosales JJ, Morales MI, Sancho L, Lozano MD, Mesa-Guzmán M and García-Velloso MJ: Diagnostic accuracy of visual analysis versus dual time-point imaging with 18F-FDG PET/CT for the characterization of indeterminate pulmonary nodules with low uptake. Rev Esp Med Nucl Imagen Mol (Engl Ed) 40: 155-160, 2020.